GEOPHYSICS

Layered deformation in the Taiwan orogen

T.-Y. Huang,[1] Y. Gung,[1*] B.-Y. Kuo,[2*] L.-Y. Chiao,[3] Y.-N. Chen[3]

The underthrusting of continental crust during mountain building is an issue of debate for orogens at convergent continental margins. We report three-dimensional seismic anisotropic tomography of Taiwan that shows a nearly 90° rotation of anisotropic fabrics across a 10- to 20-kilometer depth, consistent with the presence of two layers of deformation. The upper crust is dominated by collision-related compressional deformation, whereas the lower crust of Taiwan, mostly the crust of the subducted Eurasian plate, is dominated by convergence-parallel shear deformation. We interpret this lower crustal shearing as driven by the continuous sinking of the Eurasian mantle lithosphere when the surface of the subducted plate is coupled with the orogen. The two-layer deformation clearly defines the role of subduction in the formation of the Taiwan mountain belt.

The subduction of plate not only brings about continental or arc-continent collision but also affects mountain building in a complex way during the collision (*1*–*3*). The orogeny of Taiwan was preceded by the subduction of the Eurasian Plate (EP) eastward under the Philippine Sea plate at the Manila trench. With the consumption of the oceanic lithosphere in between, the Luzon arc approached the Eurasian continent at 4 to 5 million years ago (Ma) and initiated the collision (*4*) (Fig. 1). How the subduction of the EP interacts with the collision is a subject of debate. The thin-skinned critical taper wedge model asserts that the mountain is shaped by deformation above a detachment surface (décollement), below which the material is subducting along with the EP and intact from the collision (*5*, *6*). A thick-skinned lithospheric collision model advocates vertically continuous deformation on the lithospheric scale (*7*–*9*), thus including the subducted plate. Shear-wave splitting observations with large delay times in Taiwan, as in many other mountain belts, requires a coherent deformation, even extending to the sublithospheric mantle (*10*–*12*). This interpretation is open to question because shear-wave splitting measurements lack the adequate vertical resolution. Recently, the large-scale experiment Taiwan Integrated Geodynamics Research (TAIGER) (*8*, *9*) in the Taiwan collision zone has yielded improved observations of deformational structures in the lower crust, reinforcing the view of thick-skinned tectonics. However, this work established that deformation is not restricted to the upper crust but fails to define the deformation fabrics in details that could help to infer the interaction between the collision and subduction.

We developed three-dimensional (3D) tomographic models of shear-wave velocity (*Vs*) and its azimuthal variation for the crust of Taiwan, using the empirical Green's functions (EGF) of

[1]Department of Geosciences, National Taiwan University, Taipei, Taiwan. [2]Institute of Earth Sciences, Academia Sinica, Taipei, Taiwan. [3]Institute of Oceanography, National Taiwan University, Taipei, Taiwan.
*Corresponding author. E-mail: ycgung@ntu.edu.tw (Y.G.); byk@earth.sinica.edu.tw (B.-Y.K.)

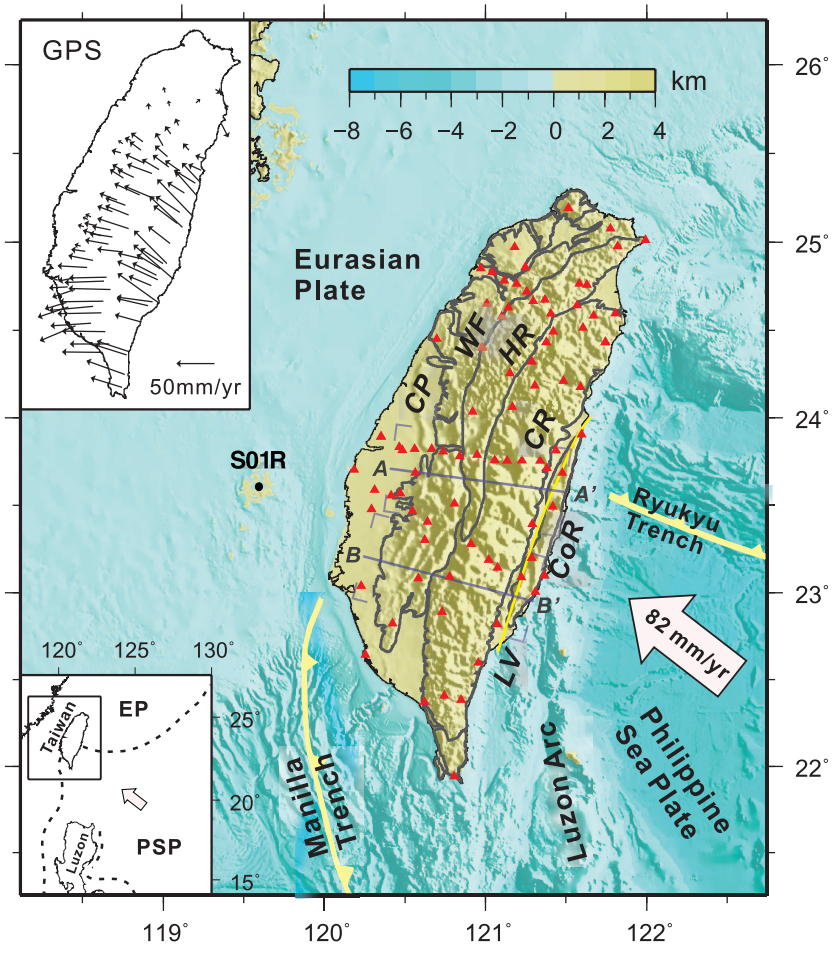

Fig. 1. The Taiwan orogen and regional plate tectonics. The convergence of the Philippine Sea plate (PSP) toward the EP at 82 mm/year (arrow) is being absorbed by the orogeny at Taiwan and the subduction at the Ryukyu trench. The GPS field (*27*) (simplified, upper left inset) illustrates the motion of the Taiwan orogen relative to the reference station S01R at the EP. Two cross sections, AA′ and BB′, sample the mature and young portions of the mountain belt (average area bracketed), respectively. Broadband seismic stations used in the ambient noise tomography are denoted by red triangles. LV, Longitudinal Valley or the suture zone; CoR, Coastal Range (*26*).

Rayleigh waves extracted from ambient seismic noises. With the unprecedented data amount and various advantages of noise-derived EGFs over conventional earthquake-based surface waves (*13*), we are able to resolve the detailed variations of seismic anisotropy from the shallow crust to about a 30-km depth. We implemented a wavelet-based multiscale inversion technique (*14*) to solve the simultaneous inversion for both isotropic and anisotropic models (*15*).

The tomographic models demonstrate that both *V*s and azimuthal anisotropy at shallow depths correlate well with the surface geology (Fig. 2). Among geological provinces of the Taiwan orogen (Fig. 1), the Coastal Plain (CP) and the Western Foothills (WF) are characterized by low *V*s, whereas the Hsuehshan Range (HR) and the Central Range (CR) are underlain by high *V*s. The fast directions of azimuthal anisotropy are generally parallel to the trend of the mountain belt, from north-to-south in southern Taiwan to northeast-to-southwest in northern Taiwan. This orogen-parallel anisotropy (OPA) may reflect the structural fabric of the brittle crust under compression, which can be the foliation of the metamorphic rocks of the HR and CR and the north-south aligned fold and thrust structures in the WF. These shallow crustal features, when combined with the teleseismic shear-wave splitting observations (*11*), support the hypothesis that orogenic processes generate the same deformational fabrics down to the sublithospheric mantle (*9*, *10*).

The close correlation of seismic properties with surface geology and structural trends diminishes with depth. At depths greater than 10 to 20 km, lower *V*s is associated with the HR and CR, and the fast axis of anisotropy aligns with the global positioning system (GPS)–indicated convergence direction. This convergence-parallel anisotropy (CPA) increases to ~30-km depth, below which the model resolution degrades. The same pattern of anisotropy may persist deeper as the azimuthal variation in the velocity of P_n, the *P* wave propagating in the uppermost mantle, exhibits similar east-west fast directions (*16*).

Two example cross sections averaging along central and southern Taiwan show variations in the fast direction of anisotropy with depth (Fig. 3). We model the high-angle rotation of anisotropy as a function of depth, using a scaled arctangent function, and define the anisotropy transition boundary (ATB) between the OPA and the CPA and the top of the CPA (fig. S4) (*15*). The ATB tilts gently from 5- to 10-km depths beneath the CP and WF to a 15-km depth beneath the CR. The CPA develops 2 to 5 km below the ATB in the upper crust in western Taiwan and in the lower crust beneath the CR. We performed resolution and recovery tests to show the robustness of a sharp ATB (Fig. 3) (*15*).

We propose that the CPA results from alignment of anisotropic minerals by subhorizontal shearing parallel to the convergence direction and that the ATB separates the compression-dominant upper crust and the shear-dominant mid- to lower crust. Amphibole, an abundant mineral in the lower crust (*17*), may be the candidate anisotropic agent potentially capable of producing high azimuthal anisotropy with fast direction parallel to shear (*18*). The lineation on subhorizontal rock cleavages aligned by shearing may also give rise to CPA (*19*). The depth distribution

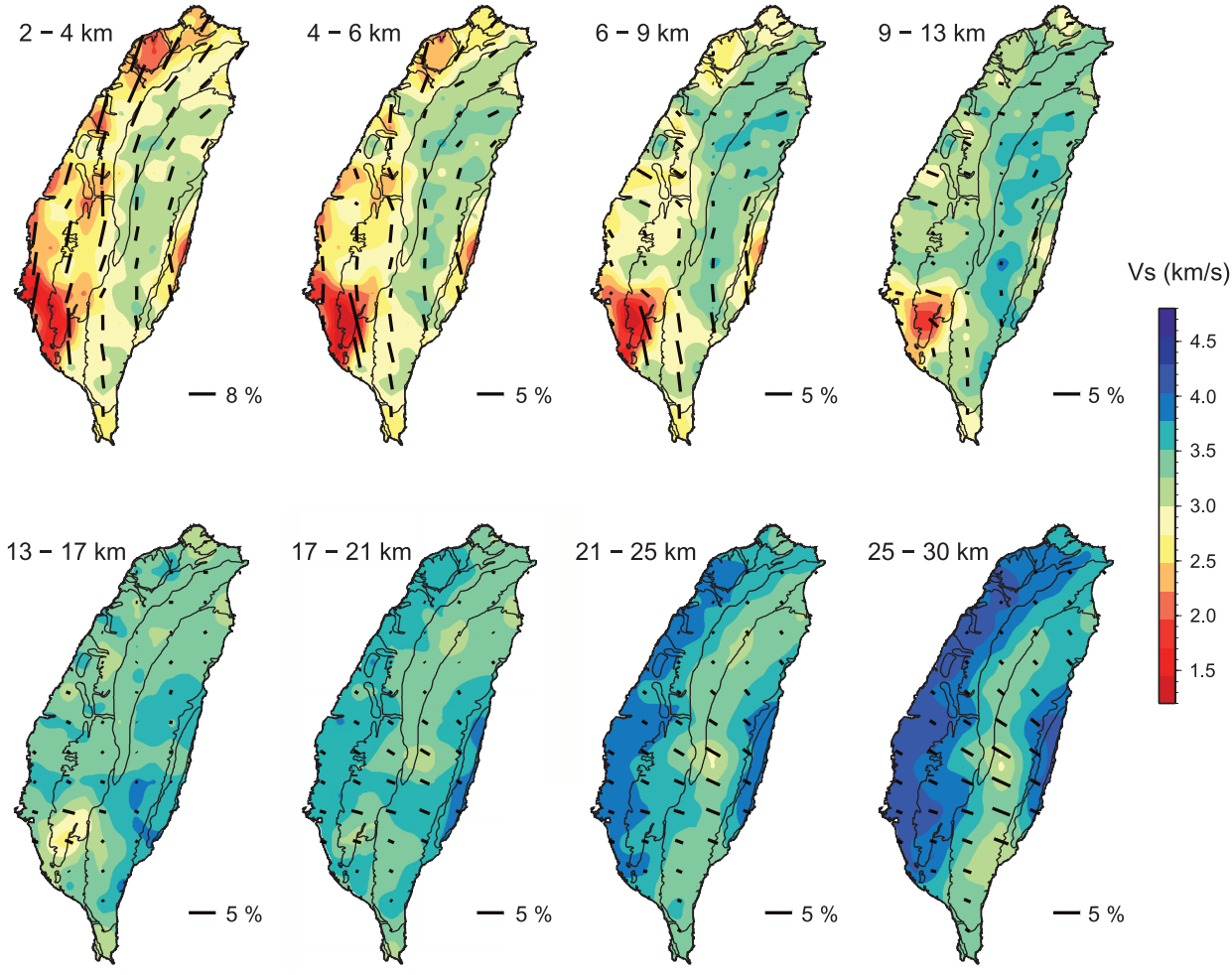

Fig. 2. Maps of *Vs* and azimuthal anisotropy at selected depths. The *Vs* in the high mountains is relatively high in the upper crust but relatively low in the lower crust. The fast direction of azimuthal anisotropy is represented by the orientation of the bar with its length proportional to the strength of anisotropy indicated in the lower right of each panel. The fast directions rotate from nearly orogen-parallel to nearly convergence-parallel across 10- to 15-km depths.

of the CPA requires shearing to occur mostly within the subducted Eurasian crust, where relative motion can be imposed between the surface of the subducted plate, where collision exerts resistance, and the continuously sinking mantle lithosphere (Fig. 4). The CPA diminishes rapidly toward northern Taiwan (Fig. 2), where subduction of the EP is absent, in agreement with the proposed subduction-induced mechanism.

The proposed shear deformation beneath the HR and CR may occur in the regime of ductile flow. In this region, with estimated temperatures (~750°C at a 25-km depth) (*20*) comparable to those suggested for the ductile lower crust of Tibet (*3*), the seismicity is considerably reduced relative to the surroundings. Below the CR, the relatively low *Vs* in the CPA zone is compatible with elevated temperatures. The magnitude of the CPA increases with depth to 30 km, implying an enhanced shear flow with increasing temperature. The viscosity below the CR at depths corresponding to the CPA zone is lower than 10^{19} from postseismic deformation (*21*), which is lower than required to maintain ductile flow in Tibet (*3*). Toward the west, the change in mineralogy at shallower depth and the elevation of the CPA zone to the brittle deformation regime may reduce the strength of the anisotropy.

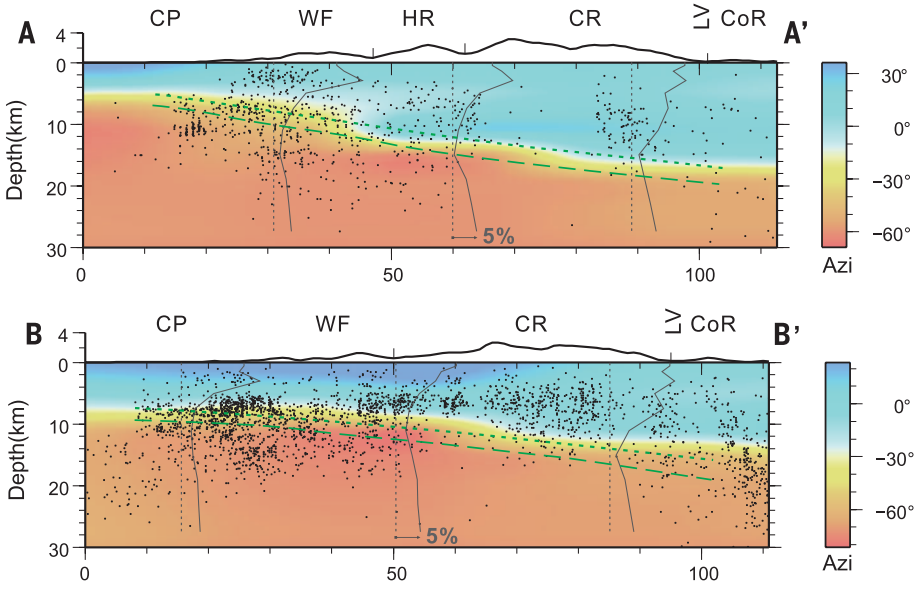

Fig. 3. Cross sections showing rotation of anisotropy fabrics with depth. The positions of AA′ and BB′ are shown in Fig. 1. The resolved fast directions of azimuthal anisotropy are color coded to highlight the rotation from 30° to 0°, to −60° to −90° over a narrow depth range. Green dotted lines represent the parameterized ATB, which in general agrees with the color description of the rotation. Green long dashed lines mark the top of the CPA zone. Both sections are decorated by seismicity during 2003 to 2007. In each section, three representative profiles of the strength of anisotropy are shown in gray lines, and the reference for zero amplitude is shown by the vertical dotted lines.

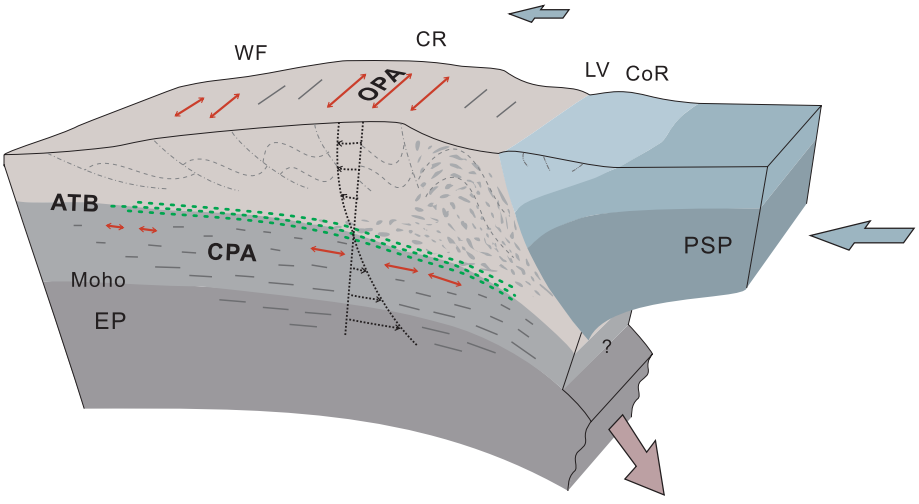

Fig. 4. Cartoon illustration of the layered deformation zones in the Taiwan orogen. The compressional tectonics and the subduction-dominated deformation are characterized by the OPA and the CPA, respectively. Red double arrows highlight the fast directions of these two sets of anisotropy. The ATB (green dots) separates the two deformation regimes and couples the upper crust of the orogen with the subduction. Light blue arrows indicate the motion of the PSP and the orogen. The brown arrow indicates the continuous sinking of the mantle lithosphere of the EP while the upper part of the plate is coupled with the orogen. The schematic velocity profile illustrates the relative motion of the collision-subduction system. The exhumation of the continental basement material beneath the CR is illustrated with irregular spindles.

The ATB averaged in central Taiwan dips more steeply (8.3°) than that in southern Taiwan (4.8°) in the range between the CP and the CR. Below the CR, the ATB is on average 5 km deeper in central than in southern Taiwan. This is compatible with the geochemical evidence that the pre-Tertiary metamorphic rocks exposed in the eastern CR (the Tananao Complex) were exhumed from the upper crust of the underthrusted continental margin (*22*). The ATB zone may initiate in the vicinity of the surface of the EP but carve into the underthrusted crust as the latter is peeled off during collision. The maximum depth of exhumation beneath the eastern CR may be constrained at the top of the CPA, at roughly a 20-km depth, where shearing fully develops. This adds a constraint on the models that incorporate deep exhumation (*23*, *24*). In southern Taiwan, where orogeny might have started but not culminated yet (*25*) and no Eurasian basement outcrops have been found (*26*), the ATB retains a smaller slope and is shallower beneath the CR.

A previous hypothesis suggested a décollement separating the upper crust from the underthrusted plate (*5*). The ATB interpreted here is related to a no-slip boundary condition between the upper and lower crustal levels. Because of this coupling, the shear zone extends into the crust and probably the mantle of the down-going plate, in contrast to the focused shear and slip along a single detachment. Some portion of the convergence may be taken up by the ductile flow across this broad shear zone. However, the layered deformation implies that the compressional tectonics is confined above the ATB, which echoes the central principle of the thin-skinned tectonics.

In the sense of the distribution of deformation, our observation is consistent with the thick-skinned tectonics (*7*–*19*). However, previous studies supportive of thick-skinned model emphasized (i) a continuous deformation to counter the concept of the décollement and (ii) a large-scale compressional deformation dominated by collision. We argue that the collision produces compressional tectonics in the upper crust of the orogen but, together with the sinking slab, induces shear within the lower crust or the crust of the subducted EP, rather than the entire crust being shortened and thickened. We speculate that the shear is an ambient state of stress of the subducted plate, which may not be easily overprinted

by the deep-penetrating faults (*8*). Our interpretation suggests that the ongoing formation of the mountain of Taiwan is coupled with the subduction through shearing. The coupling might be spatially heterogeneous and evolve in time as subduction progresses to collision.

REFERENCES AND NOTES

1. V. Schulte-Pelkum *et al*., *Nature* **435**, 1222–1225 (2005).
2. J. Nábelek *et al*., *Science* **325**, 1371–1374 (2009).
3. C. Beaumont, R. A. Jamieson, M. H. Nguyen, S. Medvedev, *J. Geophys. Res.* **109**, B06406 (2004).
4. T. Byrne *et al*., The arc-continent collision in Taiwan, in *Arc-Continent Collision, Frontiers in Earth Sciences*, D. Brown, P. Ryan, Eds. (Springer-Verlag, Berlin, 2011), pp. 213–245.
5. D. Davis, J. Suppe, F. A. Dahlen, *J. Geophys. Res.* **88**, 1153–1172 (1983).
6. S. Carena, J. Suppe, H. Kao, *Geology* **30**, 935 (2002).
7. F. Wu, R.-J. Rau, D. Salzberg, *Tectonophysics* **274**, 191–220 (1997).
8. E. A. Bertrand *et al*., *J. Geophys. Res.* **117**, B01402 (2012).
9. F. T. Wu, H. Kuo-Chen, K. D. McIntosh, *J. Asian Earth Sci.* **90**, 173–208 (2014).
10. P. G. Silver, *Annu. Rev. Earth Planet. Sci.* **24**, 385–432 (1996).
11. H. Kuo-Chen, F. T. Wu, D. Okaya, B.-S. Huang, W.-T. Liang, *Geophys. Res. Lett.* **36**, L12303 (2009).
12. W. Huang *et al*., *J. Geophys. Res.* **105** (B12), 27979–27989 (2000).
13. T.-Y. Huang, Y. Gung, W.-T. Liang, L.-Y. Chiao, L. S. Teng, *Geophys. Res. Lett.* **39**, L05305 (2012).
14. L.-Y. Chiao, B.-Y. Kuo, *Geophys. J. Int.* **145**, 517–527 (2001).
15. Materials and methods are available as supplementary materials on *Science* Online
16. C.-H. Chen, Y.-H. Chen, H.-Y. Yen, G.-K. Yu, *Earth Planets Space* **55**, 223–230 (2003).
17. R. L. Rudnick, S. Gao, Composition of the continental crust, in *Treatise of Geochemistry 2nd ed.*, H. Holland, K. Turekian, Eds. (Elsevier, Amsterdam, 2014).
18. D. J. Tatham, G. E. Lloyd, R. W. H. Butler, M. Casey, *Earth Planet. Sci. Lett.* **267**, 118–128 (2008).
19. D. Mainprice, A. Nicolas, *J. Struct. Geol.* **11**, 175–189 (1989).
20. H. Kuo-Chen *et al*., *Geophys. Res. Lett.* **39**, L22302 (2012).
21. Y.-J. Hsu, S.-B. Yu, M. Simons, L.-C. Kuo, H.-Y. Chen, *Tectonophysics* **479**, 4–18 (2009).
22. W. G. Ernst, *J. Metamorph. Geol.* **1**, 305–329 (1983).
23. M. Simoes *et al*., *J. Geophys. Res.* **112**, B11405 (2007).
24. P. Yamato, F. Mouthereau, E. Burov, *Geophys. J. Int.* **176**, 307–326 (2009).
25. Y.-H. Lee *et al*., *Geology* **43**, 451–454 (2015).
26. C.-S. Ho, *An Introduction to the Geology of Taiwan* (Central Geological Survey, Taiwan, 1999).
27. B. Rousset, S. Barbot, J.-P. Avouac, Y.-J. Hsu, *J. Geophys. Res.* **117**, B12405 (2012).

ACKNOWLEDGMENTS

We thank W.-T. Liang, F. T. Wu, K.-L. Wang, T.-F. Yui, W.-S. Chen, and J. Suppe for helpful discussions and comments. T. Byrne helped clarify the geological implications in an early draft and provided inspiring discussion. We thank three reviewers for their critical comments. We acknowledge the Taiwan Integrated Geodynamics Research (TAIGER) project, The Taiwan Earthquake Research Data Center (TECDC), Broad-Band Array in Taiwan for Seismology (BATS), and Central Weather Bureau Broad-Band array (CWBBB) for providing continuous broadband seismic waveforms. This work was supported by the Ministry of Science and Technology of Taiwan (MOST 103-2116-M-002 -026) and Academia Sinica, Taiwan (AS-104-TP-A04). All the data used in this study are available in the following websites: CWBBB: http://gdms.cwb.gov.tw/index.php; BATS: http://bats.earth.sinica.edu.tw; TAIGER: http://ds.iris.edu/mda/YM?timewindow=2006-2009.

SUPPLEMENTARY MATERIALS

www.sciencemag.org/content/349/6249/720/suppl/DC1
Materials and Methods
Supplementary Text
Figs. S1 to S12
Tables S1 and S2
References (*28*–*35*)

24 March 2015; accepted 30 June 2015
10.1126/science.aab1879

2D MATERIALS

Observation of tunable band gap and anisotropic Dirac semimetal state in black phosphorus

Jimin Kim,[1] Seung Su Baik,[2,3] Sae Hee Ryu,[1,4] Yeongsup Sohn,[1,4] Soohyung Park,[2] Byeong-Gyu Park,[5] Jonathan Denlinger,[6] Yeonjin Yi,[2] Hyoung Joon Choi,[2,3] Keun Su Kim[1,4]*

Black phosphorus consists of stacked layers of phosphorene, a two-dimensional semiconductor with promising device characteristics. We report the realization of a widely tunable band gap in few-layer black phosphorus doped with potassium using an in situ surface doping technique. Through band structure measurements and calculations, we demonstrate that a vertical electric field from dopants modulates the band gap, owing to the giant Stark effect, and tunes the material from a moderate-gap semiconductor to a band-inverted semimetal. At the critical field of this band inversion, the material becomes a Dirac semimetal with anisotropic dispersion, linear in armchair and quadratic in zigzag directions. The tunable band structure of black phosphorus may allow great flexibility in design and optimization of electronic and optoelectronic devices.

Two-dimensional (2D) atomic crystals have continued to show great potential for application in nanoscale devices (*1*). A key issue is controlling their electronic states to overcome the limit of natural properties. Graphene's effectively massless state of charge carriers is a result of the conical band structure (*2*). However, the lack of a band gap (E_g) limits the on-off current ratio in planar field-effect transistors (*3*, *4*), and it has been difficult to reliably achieve a sizable E_g without degrading its electronic quality (*5*–*7*). It would thus be desirable to realize a 2D system with a widely tunable E_g.

A potential candidate is few-layer black phosphorus (BP), a layered material of elemental phosphorus (*5*–*22*). The single-layer BP (or phosphorene) has a honeycomb network similar to graphene but is strongly puckered (armchair-shaped along x and zigzag-shaped along y in Fig. 1A), rendering its electronic state highly susceptible to external perturbations (*11*–*22*). The low-energy band structure of phosphorene can be approximated by a bonding and antibonding pair of mainly $3p_z$ orbitals (*11*, *12*). The corresponding valence band (VB) and conduction band (CB) are located at the zone center (Γ_2^+ and Γ_4^- states in Fig. 1B) with the predicted E_g of 0.7 to 1.6 eV (*13*–*17*). For multilayers, the introduction of interlayer coupling reduces E_g with increasing film thickness and reaches ~0.33 eV in bulk BP (*11*–*14*). The E_g of BP films and nanoribbons has been widely predicted to be tunable by strain (*15*–*17*) and electric field (*17*–*21*), the latter of which is more viable in gated devices. The electric field affects the real-space distribution of VB and CB states to be shifted in opposite directions to each other. Their potential difference and band mixing lead to a reduction in E_g, which is often termed the giant Stark effect (*23*–*26*). However, despite its potential importance for device applications, little is known experimentally about this effect on the surface of 2D semiconductors under a vertical electric field.

Here we report the realization of a widely tunable E_g in BP by means of the in situ deposition of potassium (K) atoms, the well-known technique to induce doping and electric field in 2D van der Waals systems (*27*). The K atoms on BP donate charges to the few top phosphorene layers, which are confined to form 2D electron gas near the surface (Fig. 1A, bottom). The band structure measured by angle-resolved photoemission spectroscopy (ARPES) at low K density is slightly n-doped with E_g greater than 0.6 eV (Fig. 1C). With increasing dopant density, the electric field from the ionized K donors gradually reduces E_g owing to the giant Stark effect, as supported by our density functional theory (DFT) calculations. Consequently, the electronic state of BP is widely and continuously tuned from a moderate-gap semiconductor to a band-inverted semimetal. At the critical dopant density of this band-inverted transition (*21*, *22*), the electronic state becomes an anisotropic Dirac semimetal (Fig. 1D). This control mechanism of E_g should work in dual-gate BP devices for precisely balancing between high mobility and moderate E_g.

Figure 1, E to H, shows a series of ARPES spectra taken along the armchair direction k_x with different dopant density near direct E_g. As expected for pristine BP (*28*, *29*), in Fig. 1E there

[1]Department of Physics, Pohang University of Science and Technology, Pohang 790-784, Korea. [2]Department of Physics, Yonsei University, Seoul 120-749, Korea. [3]Center for Computational Studies of Advanced Electronic Material Properties, Yonsei University, Seoul 120-749, Korea. [4]Center for Artificial Low Dimensional Electronic Systems, Institute for Basic Science, Pohang 790-784, Korea. [5]Pohang Accelerator Laboratory, Pohang University of Science and Technology, Pohang 790-784, Korea. [6]Advanced Light Source, Lawrence Berkeley National Laboratory, Berkeley, CA 94720, USA.
***Corresponding author. E-mail: keunsukim@postech.edu**

Layered deformation in the Taiwan orogen

T.-Y. Huang *et al.*

Science **349**, 720 (2015);
DOI: 10.1126/science.aab1879